Asociación Argentina
de Mecánica Computacional

Mecánica Computacional Vol XXVI, pp.3458-3474
Sergio A. Elaskar, Elvio A. Pilotta, Germán A. Torres (Eds.)
Córdoba, Argentina, Octubre 2007

ANODIC PH DISTRIBUTION ANALYSIS DURING ELECTROCHEMICAL TREATMENT OF TUMORS: NUMERICAL SIMULATIONS

Pablo Turjanski[a], Alejandro Soba[a], Cecilia Suarez[a], Lucas Colombo[b], Graciela González[a], Fernando Molina[c] and Guillermo Marshall[a]

[a]*Laboratorio de Sistemas Complejos, Departamento de Computación, FCEyN, Universidad de Buenos Aires, (C1428EGA) Buenos Aires, Argentina, marshallg@arnet.com.ar , http://lsc.dc.uba.ar*
[b]*Depto. de Inmunobiología, Inst. de Oncología Angel H. Roffo, Universidad de Buenos Aires, (C1417DTB) Buenos Aires, Argentina.*
[c]*INQUIMAE, FCEyN, Universidad de Buenos Aires, (C1428EHA) Buenos Aires, Argentina*

Keywords: Tumors, Electrochemical treatment, Mathematical modelling, Numerical simulation

Abstract. Electrochemotherapy (EChT) of tumors consists in the passage of a direct electric current through electrodes inserted locally in the tissue, mainly causing its necrosis. This kind of treatment has been specially applied in China for the last ten years in more than 10 000 patients with good clinical results. The extreme pH changes induced by EChT has been proposed as the main tumor destruction mechanism. In this paper, we describe two different numerical models of EChT (non-buffered and buffered models) that analyze electrolyte diffusive and migratory transport near the anode in a diluted solution, with or without the presence of buffer in the medium. These models use the quasi-one-dimensional Nernst-Planck equations under the hypothesis of electroneutrality and galvanostatic conditions. The equations are solved, for each time step, with finite differences in a fixed domain with a variable mesh that allows greater accuracy near the anodic boundary region. We compare pH distribution predictions derived from the non-buffered and the buffered models with experimental results obtained from collagen I gels and subcutaneous tumors developed in mice, respectively. Simulations predict that, after the EChT treatment, an initial condition with an homogeneous and almost neutral pH becomes extremely acid at the anode, rapidly recovering its neutral value as we move away from it. The strong acidification expands through the anodic area as the EChT dosage increases. These predictions are in good agreement with experimental results. Other qualitative and quantitative comparisons reveal that the non-buffered model has a better correlation with reality than the buffered one. This approach and results open a promising area of research that may help in the elucidation of the real consequences of an EChT applied to tumor tissues. We believe this could have significant implications in the future design of optimal operative conditions and dose planning of this kind of therapy.

1 INTRODUCTION

Bioelectromagnetics research has been extensively explored in the last thirty-five years including radiofrequency, magnetic resonance, hyperthermia and electrotherapy, among other techniques (Chou, 2007). Electrochemotherapy (EChT) of tumors, also called electrotherapy or electro-acupuncture, consists in the passage of a direct electric current through two or more electrodes inserted locally in the tissue, with the objective of destroying it (Nilsson et al., 2000b; Cabrales and Luna, 2003). This kind of treatment has been specially applied in China for the last decade in more than 10 000 patients with good clinical results (over-all response rate of 78% and five-year survival rate of 47%) (Xin, 1994b,a). The effectiveness of this treatment has been proved in different kinds of tissues, not only superficial but also deeply located (as skin, lung, liver, breast, pancreas, esophagus, maxillofacial and lingual) (Xin et al., 2001, 1997; Lin et al., 2001; Ren et al., 2001; Wu et al., 2001; Wojcicki et al., 1999; Zhang et al., 2003; Li et al., 2006). EChT is reported to be a simple, safe, less traumatic, quick recovery and low-cost technique for eliminating solid tumors. The therapy is especially indicated for patients or tumors that are unsuitable for surgery, radiotherapy or chemotherapy. It has even been suggested that EChT improves the benefits and minimize the side effects of the above mentioned therapies (Cabrales and Luna, 2003).

The EChT causes the destruction of the tumor by necrosis and apoptosis (von Euler et al., 2004). During the treatment, the anodic electrochemical reaction consists mainly in water decomposition and chloride oxidation, while protons, oxygen and chlorine are released (Berendson and Simonsson, 1994; Li et al., 1997). On the other hand, the cathodic reaction consists in the production of hydroxide ions and hydrogen, also from water decomposition. Ionic species present at the electrode periphery are transported through the medium by diffusion, migration and convection. This results in a strong anodic acidification and cathodic alcalinization, as well as a net movement of fluid from anode to cathode (Vijh, 2004). Part of the gases released at the electrodes remain present in the medium and participate in other chemical reactions with organic and inorganic components of the tissue (Nilsson et al., 2000a). These further reactions can induce the production of new toxic products and local pH changes. It has been proposed that these extreme pH changes are the main cause responsible for the tumor-mass destruction observed after the treatment and that they can reliably predict the extent of the tumor necrotic area (Finch et al., 2002; von Euler et al., 2002).

Before the EChT can be clinically applied and generalized in Occident, it is necessary to better understand its subjacent mechanisms and to develop a reliable strategy of treatment application. Mathematical modeling and numerical simulation of the process may be a good approach to achieve this point. The mathematics dedicated to the resolution of oncologic problems, called "oncologic mathematics", is considered a new interdisciplinary specialty (Preziosi, 2003; Byrne et al., 2006) and it is based in the utilization of mathematical methods and models for the description and prediction of morphologic and physiologic aspects of the tumor development. Many of these models are related to different kind of tumor therapies, as for hyperthermia therapy optimization (Tsuda et al., 1996). There are some mathematical models developed that concerns EChT (Cabrales et al., 1999; Nilsson et al., 1998, 1999, 2000a; Nilsson and Fontes, 2001; Avramov Ivic et al., 2003; Tell et al., 2004). Among them, Nilsson's models assimilate the tissue to an aqueous solution of a given ionic concentration similar to that present in normal tissues (0.16 M) (West, 1985), with or without buffer capacity and organic content. They describe (for the anode and the cathode separately) the basic electrochemical reactions involved at the electrodes and the space-temporal transport of the main ionic species involved.

In this work we extend Nilsson's results comparing simulations with data obtained from in vivo and in vitro experiments. The ultimate goal is to develop a general modeling framework which could actually predict and optimize the clinical result of an EChT applied on a specific tumor mass. This general modeling framework would need to include, among other aspects, the interaction of electrode and counter electrode, a more realistic description of the tumor tissue, more chemical reactions and/or factors relevant to the pH change and the presence of electro-osmotic fluxes.

Specifically, in this paper we present two different models, both based on transport equations of ionic species in dilute solutions and on electrode kinetics. Both are reduced to a one-dimensional problem due to the assumption of spherical symmetry. The main differences between them are their buffer capacity and the temperature of the processes. The first and simplest model has no buffer capacity and it is run at 25C. Its numerical outputs are compared with in vitro experimental data obtained at room temperature from collagen I gels prepared without buffer (we used collagen I since it is generally agreed that it is the extracellular matrix component with most influence on tissue resistance to macromolecule transport (Netti et al., 2000)). The second model has some buffer capacity represented by a bicarbonate buffer system and it is run at 37C. In this case numerical outputs are compared with in vivo experimental data obtained from subcutaneous tumors developed in mice with natural buffer capacity and subjected to a physiological temperature.

2 NUMERICAL MODEL

The analysis focuses on the physicochemical processes that occur in an aqueous ionic solution surrounding a spherical platinum anode when applying a constant direct current. The cathode is situated at a distance far enough from the anode (assumed as infinity) to ensure that cathodic reaction products do not affect the spatial domain analyzed. The electrolyte domain, denoted as Ω, is limited by inner and outer spherical boundary surfaces with the radii r_a and r_r , respectively. The inner boundary $\partial\Omega_a$ represents the surface of the spherical anode, while the outer boundary $\partial\Omega_r$ represents a spherical surface at a distance large enough from the anode to ensure a constant concentration of ionic species.

Detailed derivations of basic transport equations and electrode kinetics applied to the models are presented in Nilsson et al. The non-buffered model (Nilsson et al., 1999) includes five unknown parameters: four ionic concentrations (H^+, OH^-, Cl^- and Na^+) and the electric potential (ϕ). Consequently, five model equations must be derived in the electrolyte domain and the boundaries. The buffered model (Nilsson et al., 1998) adds one more unknown parameter: the bicarbonate (HCO_3^-) concentration.

2.1 Domain equations

Differential material balances are described by:

$$\frac{\partial c_i}{\partial t} = D_i \nabla^2 c_i + \frac{z_i}{|z_i|} u_i \nabla \cdot (c_i \nabla \phi) + R_i$$

for the species

$$i = H^+, OH^-, Cl^-, HCO_3^- \tag{1}$$

where in non-buffered model

$$R_{H^+} = R_{OH^-} = k_{w,b}c_{H_2O} - k_{w,f}c_{H^+}c_{OH^-} \tag{2}$$

$$R_{Cl^-} = 0 \tag{3}$$

and in buffered model

$$R_{H^+} = k_{w,b}c_{H_2O} + k_{B,b}c_{CO_{2(aq)}}c_{H_2O} - k_{w,f}c_{H^+}c_{OH^-} - k_{B,f}c_{H^+}c_{HCO_3^-} \tag{4}$$

$$R_{Cl^-} = 0 \tag{5}$$

$$R_{OH^-} = k_{w,b}c_{H_2O} - k_{w,f}c_{H^+}c_{OH^-} \tag{6}$$

$$R_{HCO_3^-} = k_{B,b}c_{CO_{2(aq)}}c_{H_2O} - k_{B,f}c_{H^+}c_{HCO_3^-} \tag{7}$$

Here, D denotes the diffusion coefficient, t the time, u the ionic mobility, z the number of charges carried by an ion and R the species production by an homogenous chemical reaction. $k_{w,f}$ and $k_{w,b}$ are, respectively, the forward and backward rates of water proteolysis while $k_{B,f}$ and $k_{B,b}$ denote the respective forward and backward rates of bicarbonate buffer reactions. Conservation of electric charge and the condition of electroneutrality (Eq. 8 and 9) define the two remaining domain equations:

$$\nabla \cdot \left(\sum_{i=1}^{5} |z_i| u_i c_i \nabla \phi \right) + \sum_{i=1}^{5} z_i D_i \nabla^2 c_i = 0 \tag{8}$$

$$\sum_{i=1}^{5} z_i c_i = 0 \tag{9}$$

2.2 Boundary and initial conditions

Charge transfer and mass transport at the anode surface proceed at the same rate for all species involved in the electrode reactions. For the other species, mass transport is here equal to zero. Thus:

$$-D_i(\nabla c_i \cdot \mathbf{n}) - \frac{z_i}{|z_i|} u_i c_i (\nabla \phi \cdot \mathbf{n}) = \frac{v_{ij} I_j}{n_j F}$$

$$i = H^+, Cl^-$$

$$j = I, II \tag{10}$$

$$-D_i(\nabla c_i \cdot \mathbf{n}) - \frac{z_i}{|z_i|} u_i c_i (\nabla \phi \cdot \mathbf{n}) = 0$$

$$i = OH^-, Na^+, HCO_3^- \tag{11}$$

where n is the number of electrons, **n** the outward unit normal vector, v the stoichiometric coefficient and F the Faraday's constant. i denotes the current density contributed by reaction j. I corresponds to oxygen while II to chlorine evolution reactions. Current density contributed by oxygen evolution is given by:

$$I_I = I_{0,I}\{exp\{-\frac{F(\phi + E_{eq,I})}{2RT}\} - (P_{O_2})^{\frac{1}{4}} C_{H^+} exp\{\frac{F(\phi + E_{eq,I})}{2RT}\}\} \tag{12}$$

while for chlorine evolution the analogous expression is:

$$I_{II} = I_{0,II}\{C_{Cl^-} exp\{-\frac{F(\phi + E_{eq,II})}{2RT}\} - (P_{Cl_2})^{\frac{1}{2}} exp\{\frac{F(\phi + E_{eq,II})}{2RT}\}\} \tag{13}$$

Here, $C = c/c^b$ and $P = p/p^b$, where p is the pressure and b denotes equilibrium. E is the potential difference between solid and liquid phases at equilibrium conditions, relative to a reference value and derived from the Nernst's equation. I_0 denotes the exchange current density, T the absolute temperature and R the universal gas constant. Eqs. 9, 10 and 11 plus $I = I_I + I_{II}$ provide the anode boundary conditions.

At the outer boundary, concentration and electric potential gradients are given by:

$$\nabla c_i \cdot n = 0 \tag{14}$$

$$\frac{(I \cdot \mathbf{n})}{F} + \sum_{i=1}^{5} |z_i| u_i c_i (\nabla \phi \cdot \mathbf{n}) = 0 \tag{15}$$

where I is the total current density. Initially, there are no concentration gradients throughout the electrolyte, thus at $t = 0$

$$\nabla c_i = 0 \tag{16}$$

and c_i=c_i^0. The initial potential profile is solved from the domain equations and boundary conditions (Eqs. 15 and 16 for the domain and outer boundary, while Eq. 16 and $I = I_I + I_{II}$ for the anode).

3 NUMERICAL SOLUTION AND INPUT DATA

The operator ∇ is written in spherical coordinates (Cohen Tannoudji et al., 1990) and, by assuming spherical symmetry, the model is reduced to a one-dimensional problem with the space coordinate r. Then the obtained non-linear equation system is solved by the Newton's method (Gear, 1971).

The very steep slopes of the concentration and electric potential spatial values close to the anode give rise to numerical problems. In order to avoid this, a new space coordinate (x) is introduced:

$$x = \frac{r_r}{r} \tag{17}$$

then:

$$1 \leq x \leq \frac{r_r}{r_a}$$

The transformation leads to shorter step lengths close to the anode and longer step lengths further out in the electrolyte domain. By this procedure, the finite difference approximation (Smith, 1986) is able to describe the large gradients at the anode surface. Note that the anode and infinite now change their positions: the first at the higher x values and the second at lower ones.

Example:

Let $r_a = 0.001$ and $r_r = 0.061$, then $1 \leq x \leq 61$

If we use 7 nodes ($ii = 7$), then $\triangle\ x$ = $\frac{61-1}{7-1}$ = 10

x	r	$\triangle\ x$	$\triangle\ r$	
1	0.061	10	0.055454545	$\Leftarrow$ infinite side
21	0.002904762	10	0.002640693	
31	0.001967742	10	0.00093702	
41	0.001487805	10	0.000479937	
51	0.001196078	10	0.000291726	
61	0.001	10	0.000196078	$\Leftarrow$ anode side

Table 1: x: new adimensional variable, r: radius ($r = \frac{r_r}{x}$), $\triangle\ x$: distance between x nodes and $\triangle\ r$: distance between r nodes

Note that, with this transformation, $\triangle\ r$ is smaller near the anode than far from it while $\triangle\ x$ is constant over all the mesh.

3.0.1 The operator ∇

In spherical coordinates and assuming spherical symmetry, the operator ∇ is written as $\nabla U(r) = \frac{\partial U(r)}{\partial r}$ (Cohen Tannoudji et al., 1990), where U(r) is a given function.

If $x = \frac{r_r}{r}$, applying the chain rule we obtain:

$$\nabla U(x) = \frac{\partial U(x)}{\partial x}\frac{\partial x}{\partial r}$$

We know that $x = \frac{r_r}{r} \rightarrow \frac{\partial x}{\partial r} = \frac{\partial\left(\frac{r_r}{r}\right)}{\partial r} = -\frac{r_r}{r^2}$. Replacing r by its own value in function of x that is, $r = \frac{r_r}{x}$, we obtain $\frac{\partial x}{\partial r} = -\frac{r_r x^2}{r_r^2} = -\frac{x^2}{r_r}$. Inserting this in the original equation we obtain:

$$\nabla U(x) = \frac{\partial U(x)}{\partial x}\frac{\partial x}{\partial r} = \frac{\partial U(x)}{\partial x}(-\frac{x^2}{r_r})$$

3.0.2 The operator ∇^2

Like with ∇ operator, we start writing the operator ∇^2 in spherical coordinates by assuming rotational symmetry (Cohen Tannoudji et al., 1990). Then $\nabla^2 U(r) = \frac{1}{r}\frac{\partial^2 r U(r)}{\partial r^2}$. Applying derivative rules, this can be rewritten as:

$$\nabla^2 U(r) = \frac{\partial^2 U(r)}{\partial r^2} + \frac{2}{r}\frac{\partial U(r)}{\partial r}$$

If $x = \frac{r_r}{r}$, applying the chain rule we obtain:

$$\nabla^2 U(x) = \frac{\partial U(x)}{\partial x}\frac{\partial^2 x}{\partial r^2} + \frac{\partial^2 U(x)}{\partial x^2}(\frac{\partial x}{\partial r})^2 + \frac{2}{r}\frac{\partial U(x)}{\partial x}\frac{\partial x}{\partial r}$$

We know that $\frac{\partial^2 x}{\partial r^2} = \frac{\partial^2 \left(\frac{r_r}{r}\right)}{\partial r^2} = \frac{\partial}{\partial r}\left(\frac{\partial \left(\frac{r_r}{r}\right)}{\partial r}\right) = \frac{\partial \left(-\frac{r_r}{r^2}\right)}{\partial r} = \frac{2r_r}{r^3}$. Replacing r by its own value in function of x that is, $r = \frac{r_r}{x}$, we obtain $\frac{\partial^2 x}{\partial r^2} = \frac{2r_r x^3}{r_r^3} = \frac{2x^3}{r_r^2}$. Introducing this in the original equation we obtain:

$$\nabla^2 U(x) = \frac{\partial^2 U(x)}{\partial x^2}(\frac{x^4}{r_r^2})$$

3.0.3 The time step

The time step length, Δt, is chosen in order to produce a stable numerical solution. We use a 150-nodes mesh and a $\Delta t = 0.0001$.

3.0.4 Discretization

The space derivatives are approximated by the finite difference method (Smith, 1986) and the time derivative is approximated by the trapezoidal rule (Burden and Faires, 1985). The equations are discretized for a one-dimensional mesh uniform in the space coordinate x. The mesh is chosen so that no grid points appear at the boundaries. Two imaginary grid points are introduced at one-half step lengths, $\Delta x/2$, outside the boundaries.

The domain equations have been solved iterating from the anode to the infinite. In all cases we used a simple scheme of discretization:

$$\frac{\partial U(x_i)}{\partial x} \cong \frac{U(x_{i+1}) - U(x_i)}{h} \tag{18}$$

and

$$\frac{\partial^2 U(x_i)}{\partial x^2} = \frac{U(x_{i+1}) - 2U(x_i) + U(x_{i-1})}{h^2} \tag{19}$$

3.0.5 Total current density

I_i (Eq. 15)is the total current density at the i node. Note that, in a sphere, if the total current density at the anode is I_a, then this density diminishes as we move away from it. Then we have:

$$I_i = \frac{I_a * Area_a}{Area_i}$$

And for a sphere:

$$I_i = \frac{I_a 4\pi r_a^2}{4\pi r_i^2} = \frac{I_a r_a^2}{r_i^2}$$

3.0.6 Electric potential (ϕ)

Having $\frac{\partial\phi(x)}{\partial x}$ for all the mesh, and the ϕ value at the anode position, we obtain $\phi(x_i)$ for the rest of the mesh by:

$$\phi(x_i) = \phi(x_{i+1}) - \frac{\partial\phi(x_i)}{\partial x} * h$$

3.0.7 Input data

Table 2 and Table 3 show the parameter values used in the non-buffered and buffered models, respectively.

Parameter	Value
$r_a\ (m)$	0.001
$r_r\ (m)$	0.061
ii	150
$k\ (s)$	0.0001
$T\ (K)$	298
$F\ (A \cdot s \cdot mol^{-1})$	96485.3415
$R\ (kg \cdot m^2 \cdot K^{-1} \cdot mol^{-1} \cdot s^{-2})$	8.31
$c^0_{H^+}$(M)	$1 \cdot 10^{-7}$
$c^0_{OH^-}$(M)	$1 \cdot 10^{-7}$
$c^0_{Cl^-}$(M)	0.160
$c^0_{Na^+}$(M)	0.160
c_{H_2O}(M)	55.5
$k_{w,f}\ (M^{-1}s^{-1})$	$1.5 \cdot 10^{11}$
$k_{w,b}\ (s^{-1})$	$2.7 \cdot 10^{-5}$
$D_{H^+}\ (cm^2s^{-1})$	$9.31 \cdot 10^{-5}$
$D_{OH^-}\ (cm^2s^{-1})$	$5.26 \cdot 10^{-5}$
$D_{Cl^-}\ (cm^2s^{-1})$	$2.03 \cdot 10^{-5}$
$D_{Na^+}\ (cm^2s^{-1})$	$1.33 \cdot 10^{-5}$
$I\ A \cdot m^{-2}$	795.7747
$I_{0,I}\ (Am^{-2})$	$1.0 \cdot 10^{-6}$
$I_{0,II}\ (Am^{-2})$	$1.0 \cdot 10^{1}$
$E^0_I\ (V)$	$1.23 \cdot 10^{-3}$
$E^0_{II}\ (V)$	$1.36 \cdot 10^{-3}$

Table 2: In silico non-buffered model

3.0.8 Application

The software was programmed in C++ using the gsl/gsl_multiroots library (http://www.gnu.org/software/gsl/) to solve the non-linear equation system at the anode.

Parameter	Value
$r_a\ (m)$	0.001
$r_r\ (m)$	0.061
ii	150
$k\ (s)$	0.0001
$T\ (K)$	310
$F\ (A \cdot s \cdot mol^{-1})$	96485.3415
$R\ (kg \cdot m^2 \cdot K^{-1} \cdot mol^{-1} \cdot s^{-2})$	8.31
$c^0_{H^+}$(M)	$1 \cdot 10^{-7.4}$
$c^0_{OH^-}$(M)	$1 \cdot 10^{-6.2}$
$c^0_{Cl^-}$(M)	0.133
$c^0_{Na^+}$(M)	0.160
$c^0_{HCO_3^-}$(M)	0.027
c_{H_2O}(M)	55.5
$k_{w,f}\ (M^{-1}s^{-1})$	$1.5 \cdot 10^{11}$
$k_{B,f}\ (M^{-1}s^{-1})$	$3.1 \cdot 10^5$
$k_{w,b}\ (s^{-1})$	$6.7889 \cdot 10^{-5}$
$k_{B,b}\ (s^{-1})$	$6.0039 \cdot 10^{-6}$
$D_{H^+}\ (cm^2s^{-1})$	$12.5 \cdot 10^{-5}$
$D_{OH^-}\ (cm^2s^{-1})$	$7.05 \cdot 10^{-5}$
$D_{Cl^-}\ (cm^2s^{-1})$	$2.72 \cdot 10^{-5}$
$D_{Na^+}\ (cm^2s^{-1})$	$1.78 \cdot 10^{-5}$
$D_{HCO_3^-}\ (cm^2s^{-1})$	$1.49 \cdot 10^{-5}$
$I\ A \cdot m^{-2}$	795.7747
$I_{0,I}\ (Am^{-2})$	$1.0 \cdot 10^{-6}$
$I_{0,II}\ (Am^{-2})$	$1.0 \cdot 10^1$
$E^0_I\ (V)$	$1.23 \cdot 10^{-3}$
$E^0_{II}\ (V)$	$1.36 \cdot 10^{-3}$

Table 3: In silico buffered model

4 EXPERIMENTAL PROTOCOLS

4.1 Animals and tumors

The M2 cell line (mammary adenocarcinoma developed at the Research Institute "Angel H. Roffo") was injected subcutaneously by trocar in BALB/c 3-month-old female mouse. This kind of cell line is well characterized and has relatively low necrosis development and metastatic ability. EChT of solid tumors was practiced when they reached a volume of around 2 cm^3. All animals were maintained in accordance with ethics, current regulations and standards of the NIH.

4.2 EChT and pH measurement in tumors

Animals were randomly divided into 3 treatment groups. Each group was treated, under general anesthesia (intraperitoneal Ketamina-Silacine solution, 0,01 ml/g), with different Coulomb dosages of direct constant current: 10 C (10 mA, 17 min), 30 C (17 mA, 29 min) and 50 C (20 mA, 42 min). These dosages were chosen based upon previous published data (Ciria et al.,

2004). A platinum punctual electrode (anode), with a diameter of 1 mm, was inserted in the center of the tumor while the cathode was placed subcutaneously far away from it. Current was applied by means of a constant-current power supply (Consort). Both current and voltage were continuously monitored. To avoid muscle twitching, linear current ramps with a length of 2 min were applied at the beginning and at the end of the treatment.

After EChT, mice were euthanized and the tumor was longitudinally cleaved in half, along the electrode insertion plane. pH measurements were done by means of a micro-combination electrode (PHR-146, Lazar Research Lab, Inc., LA, California) with a tip diameter of 1.5 mm. Measurements were made at the anode and every 2 mm from it to the periphery of the tumor (including some healthy tissue) on a line perpendicular to the electrode. All measurements were made between 5-10 min. after current cutdown to avoid signifficant pH changes. Results were obtained from 5 independent experiments with 3 mice per group in each one (total: 15 mice per group) and were statistically analized by an ANOVA of repeated measures.

4.3 EChT and pH measurement in collagen I gels

Collagen I was diluted in distilled water at two different concentrations (30 mg/ml and 50 mg/ml) and allowed to gelificate. This preparation has no buffer. Both concentrations were chosen in order to simulate the extracellular matrix content of tumors of different consistency (from denser ones as subcutaneous to softer ones as brain tumors (Pluen et al., 2001)). Then EChT was applied at room temperature at three different Coulomb dosages: 3 C (10 mA, 5 min), 10 C (10 mA, 17 min) and 30 C (17 mA, 29 min). Two platinum punctual electrodes, with a diameter of 1 mm, were inserted in the center of the gel 3 cm far away from each other. Current was applied by means of a constant-current power supply (Consort). Both current and voltage were continuously monitored. At the end of the treatment, the pH gradient was measured by a micro-combination electrode (PHR-146, Lazar Research Lab, Inc., LA, California) with a tip diameter of 1.5 mm. Measurements were made at the anode and every 2 mm from it to the periphery of the gel. All measurements were made between 5-10 min. after current cutdown to avoid signifficant pH changes. Results were obtained from 5 independent experiments and were statistically analized by an ANOVA of repeated measures.

5 RESULTS AND DISCUSSION

5.1 Non-buffered model and in vitro experiments

Fig 1 presents simulated predictions derived from the non-buffered numerical model related to ion concentration distribution after different dosages (3, 10 and 30 coulombs) of EChT. These distributions will chemically determine the final pH distributions presented in Fig 2.

Fig 2 presents experimental in vitro results obtained from pH measurements made after different dosages (3, 10 and 30 coulombs) of EChT applied on collagen gels of 50 mg/ml (under no-buffer conditions and 25C), and compares them with simulated predictions derived by the non-buffered numerical model below the same conditions. Statistical analysis of experimental results indicates that there are significative differences between dosages applied ($p=0.0001$) and between distances from the anode ($p \leq 0.00001$) but not between gel concentrations ($p \geq 0.05$, data not shown).

Comparisons between experimental and simulated results show good qualitative but poor quantitative agreement. Both types of curves present similar slopes at the EChT dosages studied. Also, as the dosage increases, both reveal an increment in the acidic area around the anode and need a larger distance to reach a plateau (steady state) phase.

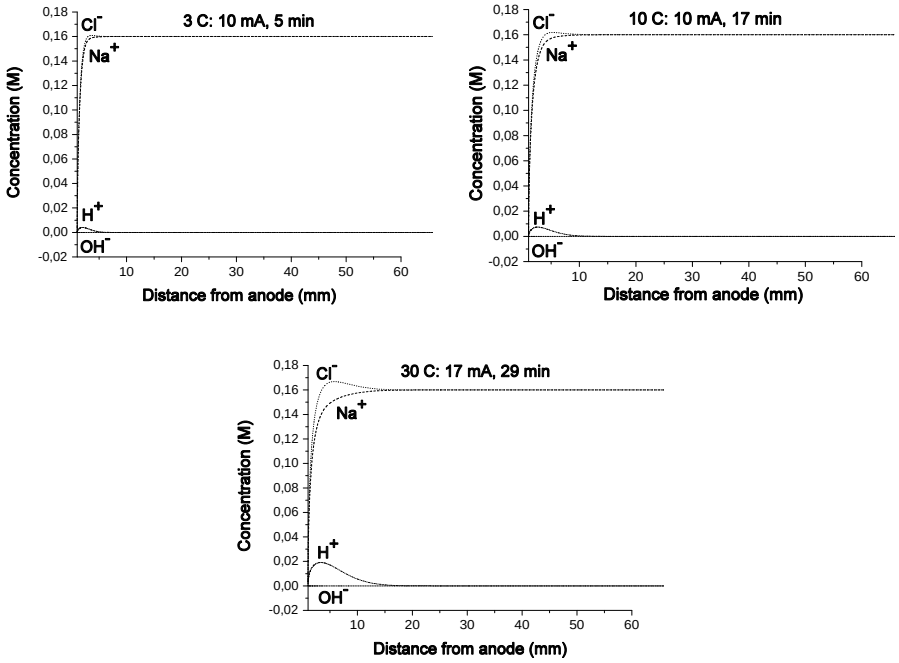

Figure 1: Non-buffered model simulations of sodium, chloride, hydrogen, hydroxile and bicarbonate ion concentration as a function of r after different dosages (3, 10 and 30 C) of EChT.

Quantitative differences consist mainly on specific pH values reached at the anode and at the plateau phase, which are higher in simulated curves than in experimental ones. Experimental pH values below 0 must be taken with great care because of technical errors present when measuring at these extreme points (due to pH meter dynamical range limitations), their inclusion here is to record the actual values indicated by the pH meter. Nevertheless, experimental pH values around the anode are still lower than simulated ones.

The acidic distilled water used for making the gels without the presence of any kind of buffer yields not really neutral experimental pH values (pH=7) at the plateau phase but rather acidic ones (pH around 4-5). Since these pH values coincide with the original values all over the gel before treatment, for practical purposes, we consider them the ”neutral” values of the system.

Assuming, as previously discussed, that ion transport is solely governed by diffusion and migration, when the electric circuit is closed species concentration fronts emerge from the electrode and advance in outward direction. Then a pH front emanating from the anode moves towards the cathode with a velocity proportional to the proton mobility times the electric field. Fig 3 shows the time evolution of the front corresponding to a pH=5 (critical value for determining cell viability and necrosis (von Euler et al., 2001, 2002)) with the application of 10 mA. Front tracking analysis reveals that pH front scales as $t^{1.00}$, for a time range between 140 and 240 sec after current startup. From this point up to 900 sec, motion slows down and scales as $t^{0.56}$). This would indicate that, from the 240 sec upwards, the motion is governed mainly by diffusion while before this time, motion could have other components such as a migratory one or a component derived from the reaction term (see material balances equation). These results correspond with those theoretically expected, as migration tends to be stronger near the electrode while diffusion would dominate far away from it. Nevertheless, more experimental data would be needed to corroborate these findings.

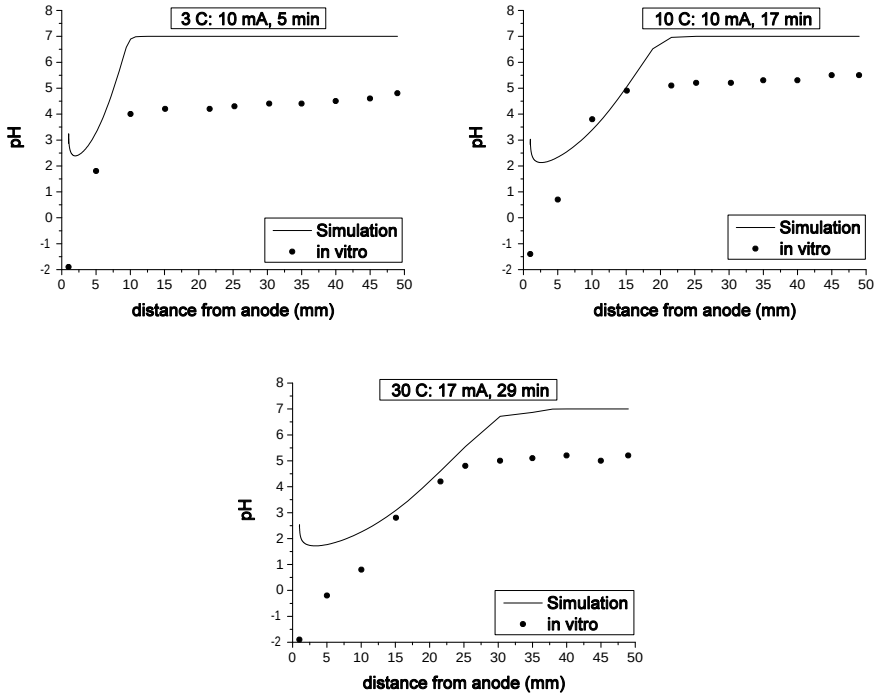

Figure 2: Spatial pH profiles obtained by the non-buffered model or after an EChT applied at different dosages (3, 10 and 30 C) to collagen I gels (50 mg/ml).

5.2 Buffered model and in vivo experiments

Fig 4 presents simulated predictions derived from the buffered numerical model related to ion concentration distribution after different dosages (10, 30 and 50 coulombs) of EChT. These distributions will chemically determine the final pH distributions presented in Fig 5.

Fig 5 presents experimental in vivo results obtained from pH measurements made after different dosages (10, 30 and 50 coulombs) of EChT applied on solid subcutaneous tumors developed in mice, and compares these results with simulated predictions derived by the buffered numerical model at 37C. Statistical analysis of experimental results indicates that there are significative differences between distances from the anode ($p \leq 0.00001$) but not between dosages ($p=0.08$).

Comparison between experimental and simulated curves show that they are qualitatively different. The main difference consists in the curve shape: a large defined step-like pH increment in the simulations but a smooth pH increment in tissues. Like simulated curves, experimental ones also seem to reach a plateau phase although a better definition of it could have been obtained if measurements were continued for a larger distance.

As shown for the non-buffered model, specific pH values at the anode are higher in simulated curves than in experimental ones. The same considerations previously discussed are valid here. On the contrary, maximum pH values obtained are more similar between both types of curves than in the non-buffered model, probably due to more similar initial conditions (physiological tissue pH is around 7.4 although in this type of tumor basal pH was rather basic).

As expected, differences between buffered model predictions and experimental results in tumor tissues are important. The main reason is that the numerical model treats the tissue as an homogeneous aqueous solution with some buffer capacity of inorganic origin (the bicarbonate system), which is unrealistic. The tumor tissue is a very complex heterogeneous solid/viscous

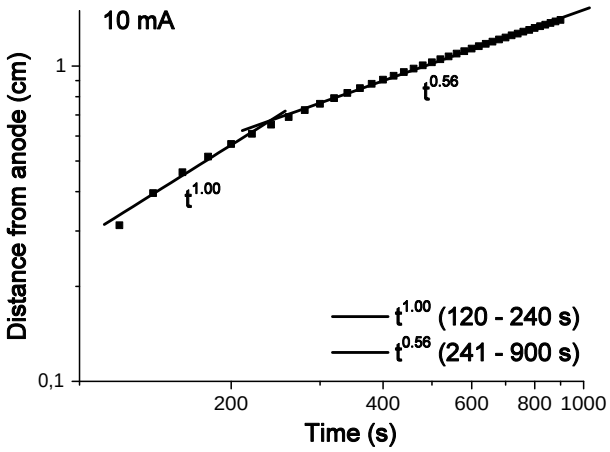

Figure 3: pH=5 front tracking obtained by the non-buffered model with the application of 10 mA.

solution mixture with more buffer capacity than that surveyed by inorganic sources. Protein content also adds great buffer capacity, in this case from an organic source. On the other hand, some tissular organic contents are susceptible to reactions with chlorine, which can originate more protons and tissue acidification (Nilsson et al., 2000a). So more realistic numerical models must take into account, among others, all these factors in order to achieve better predictions of pH spatial distribution after an EChT treatment applied on a tumor tissue.

6 CONCLUSIONS

In this work we described two different numerical models of EChT (non-buffered and buffered models) that analyze electrolyte diffusive and migratory transport near the anode in a diluted solution, with or without the presence of buffer in the medium. The system is solved, for each time step, by a finite differences technique in a fixed domain and with a variable grid that allows greater accuracy near the anodic boundary region. Numerical predictions were compared with experimental results derived from in vitro and in vivo experiments. Qualitative and quantitative comparisons reveal that the non-buffered model correlates better with reality than the buffered one.

The main goal of this paper is to make explicit the numerical resolution of Nilssons models. We detailed the parameter values and the discretization method that make the models function. We also extend their mathematical results simulating the pH front tracking (essential issue for future therapeutical predictions) and validated them with new experimental data obtained from real tumor tissues and collagen I gells, a good aproach to an extracelular matrix medium.

We believe this approach and results open a promising area of research that may help in the elucidation of the real consequences of an EChT applied to tumor tissues. This could have significant implications in the future design of optimal operative conditions and dose planning of this kind of therapy.

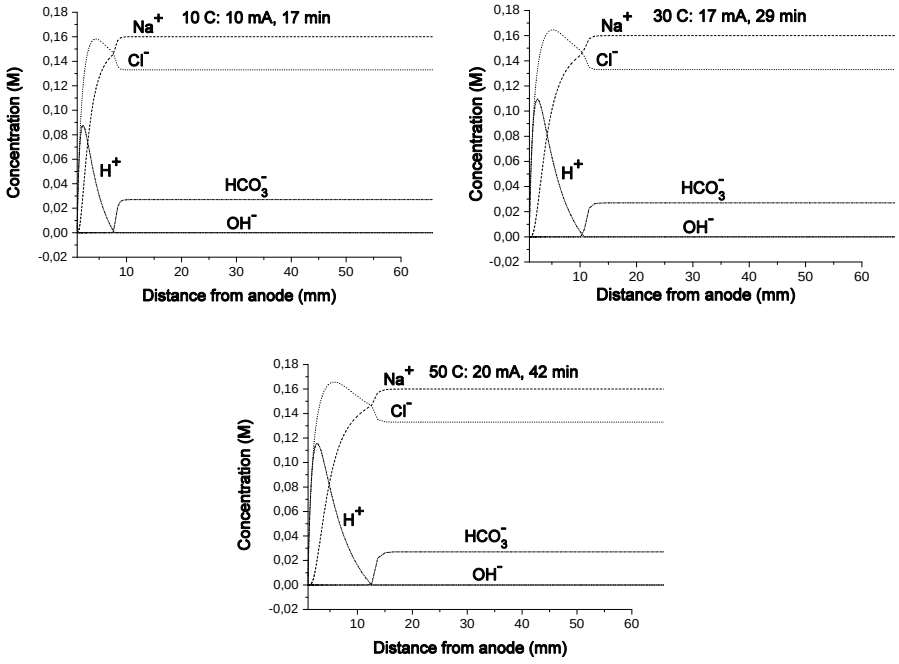

Figure 4: Buffered model simulations of sodium, chloride, hydrogen, hydroxile and bicarbonate ion concentration as a function of r after different dosages (10, 30 and 50 C) of EChT.

7 ACKNOWLEDGEMENTS

L. C., G. G., G. M. and F. M. are investigators at the Consejo Nacional de Investigaciones Científicas y Técnicas (CONICET). C. S. has a post-doctoral scholarship from the Agencia Nacional de Promoción Científica y Técnica (ANPCyT). A. S. is partially supported by University of Buenos Aires (UBA). P. T. has a scholarship from CONICET. This work was partially supported by grants from UBACyT X122/04, ANPCyT: PICTR 184, CONICET: PIP 379/98.

REFERENCES

Avramov Ivic M., Petrovic S., Zivkovic P., Nikolic N., and Popov K. An electrochemical illustration of the mathematical modelling of chlorine impact and acidification in electrochemical tumour treatment and its application on an agar-agar gel system. *Journal of Electroanalytical Chemistry*, 549:129–135, 2003.

Berendson J. and Simonsson D. Electrochemical aspects of treatment of tissue with direct current. *Eur J Surg Suppl*, 574:111–115, 1994.

Burden R. and Faires J. *Numerical analysis*. Prindle, Weber & Schmidt Boston, Mass, 1985.

Byrne H., Alarcon T., Owen M., Webb S., and Maini P. Modelling aspects of cancer dynamics: a review. *Philos Transact A Math Phys Eng Sci*, 364(1843):1563–1578, 2006.

Cabrales B., Ciria C., Bruzn P., Aldana H., Gonzlez M., Reyes F., and Delgado B. Influencia de la accin citotxica de la corriente elctrica directa en la interaccin del hospedero con las clulas cancerosas. *Revista Mexicana de Ingeniera Biomdica*, XX (4):97–103, 1999.

Cabrales L. and Luna L. La electroterapia: una alternativa terapéutica para el tratamiento de tumores. *Revista Cubana de Medicina*, 42 (6), 2003.

Chou C. Thirty-five years in bioelectromagnetics research. *Bioelectromagnetics*, 28(1):3–15, 2007.

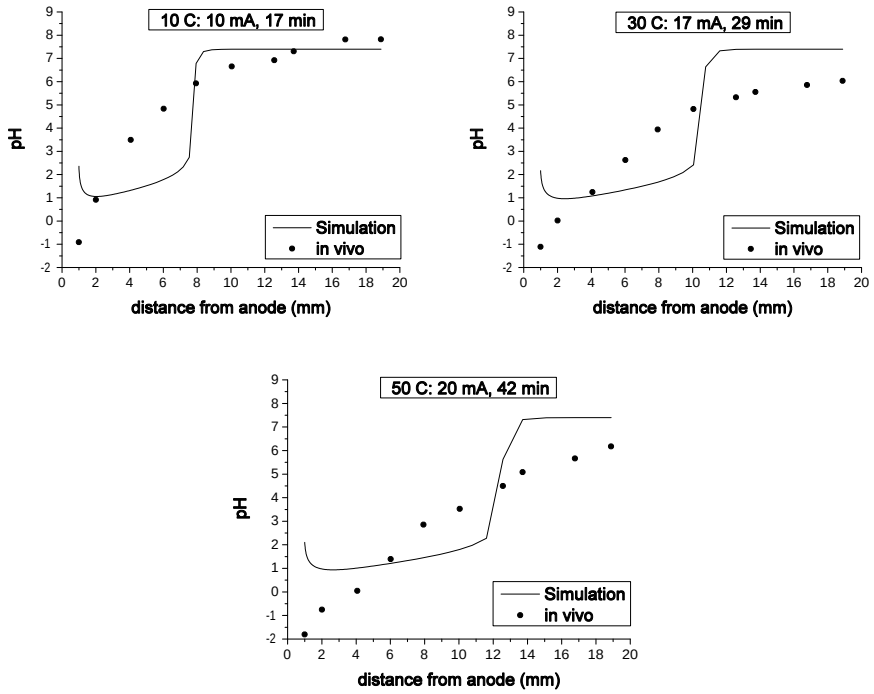

Figure 5: Spatial pH profiles obtained by the buffered model or after an EChT applied at diferent dosages (10, 30 and 50 coulombs) to subcutaneous tumors developed in mice.

Ciria H., Quevedo M., Cabrales L., Bruzon R., Salas M., Pena O., Gonzlez T., Lpez D., and Flores J. Antitumor effectiveness of different amounts of electrical charge in ehrlich and fibrosarcoma sa-37 tumors. *BMC Cancer*, 4 (1):87, 2004.

Cohen Tannoudji C., Diu B., and Laloe F. *Quantum Mechanics*, volume 2. 1990.

Finch J., Fosh B., Anthony A., Slimani E., Texler M., Berry D., Dennison A., and Maddern G. Liver electrolysis: ph can reliably monitor the extent of hepatic ablation in pigs. *Clin Sci (Lond)*, 102(4):389–395, 2002.

Gear C. *Numerical Initial Value Problems in Ordinary Differential Equations*. Prentice Hall PTR Upper Saddle River, NJ, USA, 1971.

Li J., Xin Y., Zhang W., Liu J., and Quan K. Effect of electro-acupuncture in treating patients with lingual hemangioma. *Chin J Integr Med*, 12(2):146–149, 2006.

Li K., Xin Y., Gu Y., Xu B., Fan D., and Ni B. Effects of direct current on dog liver: possible mechanisms for tumor electrochemical treatment. *Bioelectromagnetics*, 18(1):2–7, 1997.

Lin X., Jen C., Sung M., Lin J., Chou C., and Luo C. Electrochemical therapy-comparison with other local treatment methods on rat model. *Hepatogastroenterology*, 48(37):91–94, 2001.

Netti P., Berk D., Swartz M., Grodzinsky A., and Jain R. Role of extracellular matrix assembly in interstitial transport in solid tumors. *Cancer Research*, 60:2497–2503, 2000.

Nilsson E., Berendson J., and Fontes E. Development of a dosage method for electrochemical treatment of tumours: a simplified mathematical model. *Bioelectrochemistry and Bioenergetics*, 47:11–18, 1998.

Nilsson E., Berendson J., and Fontes E. Electrochemical treatment of tumours: a simplified mathematical model. *Journal of Electroanalytical Chemistry*, 460:88–99, 1999.

Nilsson E., Berendson J., and Fontes E. Impact of chlorine and acidification in the electrochemical treatment of tumours. *Journal of Applied Electrochemistry*, 30(12):1321–1333, 2000a.

Nilsson E. and Fontes E. Mathematical modelling of physicochemical reactions and transport processes occurring around a platinum cathode during the electrochemical treatment of tumours. *Bioelectrochemisty*, 53:213–224, 2001.

Nilsson E., von Euler H., Berendson J., Thorne A., Wersall P., Naslund I., Lagerstedt A., Narfstrom K., and Olsson J. Electrochemical treatment of tumours. *Bioelectrochemistry*, 51:1–11, 2000b.

Pluen A., Boucher Y., Ramanujan S., McKee T., Gohongi T., di Tomaso E., Brown E., Izumi Y., Campbell R., Berk D., and Jain R. Role of tumor-host interactions in interstitial diffusion of macromolecules: cranial vs subcutaneous tumors. *Proccedings of the National Academy of Sciences*, 98 (8):4628–4633, 2001.

Preziosi L. *Cancer Modelling and Simulation*. 2003.

Ren R., Vora N., Yang F., Longmate J., Wang W., Sun H., Li J., Weiss L., Staud C., McDougall J., and Chou C. Variations of dose and electrode spacing for rat breast cancer electrochemical treatment. *Bioelectromagnetics*, 22 (3):205–211, 2001.

Smith G. *Numerical Solution of Partial Differential Equations: Finite Difference Methods*. Oxford University Press, 1986.

Tell M., Dias G., FV S., Oliveira L., and Oliveira R. Dogs cancerous mammary glands treated by dc current: mathematical model. *URSI EMTS*, pages 519–521, 2004.

Tsuda N., Kuroda K., and Suzuki Y. An inverse method to optimize heating conditions in rf-capacitive hyperthermia. *IEEE Trans Biomed Eng*, 43 (10):1029–1037, 1996.

Vijh A. Electrochemical treatment (ect) of cancerous tumours: necrosis involving hydrogen cavitation, chlorine bleaching, ph changes, electroosmosis. *International Journal of Hydrogen Energy*, 29:663–665, 2004.

von Euler H., Nilsson E., Olsson J., and Lagerstedt A. Electrochemical treatment (echt) effects in rat mammary and liver tissue. in vivo optimizing of a dose-planning model for echt of tumours. *Bioelectrochemistry*, 54:117–124, 2001.

von Euler H., Soderstedt A., Thorne A., Olsson J., and Yongqing G. Cellular toxicity induced by different ph levels on the r3230ac rat mammary tumour cell line: an in vitro model for investigation of the tumour destructive properties of electrochemical treatment of tumours. *Biolectrochemistry*, 58:163–170, 2002.

von Euler H., Strahle K., Thorne A., and Yongqing G. Cell proliferation and apoptosis in rat mammary cancer after electrochemical treatment (echt). *Bioelectrochemistry*, 62:57–65, 2004.

West J. *Physiological basis of medical practice, 11th edition*. 1985.

Wojcicki M., Kostyrka R., Kaczmarek B., Kordowski J., Romanowski M., Kaminski M., Klonek J., and Zielinski S. Electrochemical therapy in palliative treatment of malignant dysphagia: a pilot study. *Hepatogastroenterology*, 46(25):278–284, 1999.

Wu G., Zhou X., and Huang M. Electrochemical therapy and implanted ports treatment for unresectable carcinoma of body and tail of pancreas. *Zhonghua Wai Ke Za Zhi*, 39 (8):596–598, 2001.

Xin Y. Advances in the treatment of malignant tumours by electrochemical therapy (ect). *Eur J Surg Suppl*, 574:31–35, 1994a.

Xin Y. Organization and spread of electrochemical therapy (echt) in china. *Eur J Surg*, Suppl 574:25–30, 1994b.

Xin Y., Liu D., and Meng X. Clinical observation on effect of electroacupuncture therapy in treating superficial tumor. *Zhongguo Zhong Xi Yi Jie He Za Zhi*, 21(3):174–176, 2001.

Xin Y., Xue F., and Zhao F. Effectiveness of electrochemical therapy in the treatment of lung

cancers of middle and late stage. *Chin Med J*, 110 (5):379–383, 1997.

Zhang W., Xin Y., and Zhao H. Observation on effect of electro-acupuncture in treating maxillofacial hemangioma. *Zhongguo Zhong Xi Yi Jie He Za Zhi*, 23(5):341–343, 2003.